Roller bearing under high loaded oscillations: Life evolution and accommodation mechanisms

F. Cavacece, Lucas Frache, Davide Tonazzi, Nathalie Bouscharain, David Philippon, Gwenolé Le Jeune, Francesco Massi, Yves Maheo

Roller bearing under high loaded oscillations: life evolution and accommodation mechanisms

F. Cavacece[a], L. Frache[b], D. Tonazzi[a], N. Bouscharain[b], D. Philippon[b], G. Le Jeune[c], Y. Maheo[c], F. Massi[a]

[a]University of Rome 'La Sapienza', Department of Mechanical and Aerospace Engineering, via Eudossiana 18, 00184 Rome, Italy
[b]University of Lyon, INSA-Lyon, LaMCoS, UMR5259, F-69621 Villeurbanne, France
[c]SKF Aerospace, 29 chemin de Thabor CS90114, 26904, Cedex 9, Valence, France

Abstract

High loaded oscillating bearings are used on several industrial fields such as robotics, wind power, aeronautics and aerospace. These bearings are subjected to extremely high local contact pressures and relatively low oscillatory speed. In this work, endurance tests on commercial single row spherical roller bearings enable to propose a degradation scenario for the bearing lifecycle. Topographical analyses carried out at each phase of the bearing life allowed to understand the degradation evolution at the interface between the inner-ring raceway and rolling elements. The analysis of the experimental results, with the support of numerical stress analysis, led to the understanding of the involved accommodation mechanisms. Then, a comparison with the wear processes in deep-groove ball bearings is provided.

1. Introduction

Rolling contacts between the rolling elements and raceways guarantee to support load while permitting, with the lowest possible friction losses, the relative rotation between two solids of the mechanical system [1] [2] [3]. Nowadays, bearings are expected to support extreme working conditions. In fact, the unceasing increase of both design optimization and system power transmitted involve a reduction of the contact surfaces between contacting pairs and extremal local contact solicitations [4] [5] [6].

The analysis is here focused on high loaded oscillating bearings. These working conditions are specific to aeronautical, naval and aerospace applications. High load leads to extreme contact pressures [7] between rollers and raceways, mainly of the inner-ring, while the slow oscillating motion causes repetitive mechanical solicitations on surfaces [8] combined with a variable way and speed of rotation.

Due to these operating conditions, the circulation of a lubricant and the establishment of a full elasto-hydrodynamic film can't be fully assured. A grease lubrication has to be employed; the thickener hold the oil near to the contact and then releases it under specifics conditions like high pressure, even in very low speed regimes [9] [10] . It is supposed to assure a better lubrication than oil [11] [12] [13], at least for full rotation motion.

In literature, models have been proposed to describe continuous rolling bearing damage evolution [14] [15] [16] [17] [18] [19]. During bearing lifetime, the damage evolves and there is a transition from a commercially acceptable rate to an unacceptable one. Voskamp [15], analyzing the topography of the rolling contact subsurface, has identified three fundamental steps in bearing damage evolution: running-in,

steady-state and instability. El-Thalji [14] proposed a more detailed model of bearing damage scenario, which consists in five phases: running-in, steady-state, damage initiation, damage evolution and damage growth.

However, these models don't represent all the operative conditions and cannot fully account for the interaction and the competition of the different mechanisms at the origin of the damage [5].

On the other hand, oscillating and discontinuous motion bearings have been not much investigated in the literature and only few works are addressed to these working conditions. Some models have been derived for oscillating motions to estimate the rolling bearing lifetime [20] [21]. Berthier et al. [22], performing an experimental analysis on oscillating journal bearings, highlighted the complexity of the degradation scenarios, the role of the third body flows and the existence of more than one wear mechanism. Friction and wear are largely affected by the rheology of the third-body at the contact [23] [24].

Recently, some studies on high loaded oscillating ball bearings have been carried out [5] [6] [8] [22] [25].

In [6] , the evolution of greased and ungreased contact surfaces over the bearing whole lifetime has been investigated. These studies demonstrate the role of the grease that increases considerably the bearing lifetime, protecting the bearing contacting surfaces from further superficial damage. It has been established that the failure of that ball bearings is caused by the accumulation of plastic deformations in the subsurface of the most loaded balls, while the raceways is preserved by the third body. In [5], a 3D finite element model has succeeded in evaluating the stress and strain distributions at the contact interface in deep-groove ball bearings. Its simulations confirmed the experimental results obtained in [6] : a sub-surface stress and strain zone in the ball has been observed, and a plasticization of the inner ring raceway as well. In [25], under the same boundary conditions, experimental tests on hybrid deep-groove ball bearing has been achieved. The use of a hard-ceramic balls instead of softer steel balls enables to enhance the bearing lifetime and modifies the failure mode, caused now by the destruction of the inner ring raceway surface by the ceramic balls. The comparison between hybrid and steel-steel bearings has shown how bearing materials can modify accommodation mechanisms within bearing lifecycle and so its lifetime.

In this context, this work focuses on high-loaded oscillating roller bearings. The aim is to identify the accommodation mechanisms involved during the roller bearing whole life, in order to build the degradation scenarios. A comparison between the results of this work and previous ones is then performed, in order to analyze the tribological response of different technologies operating under the same oscillating high loaded conditions.

First, the experimental set-up and the methodology is presented; then, the results of the experimental campaign are presented, analyzing the curves of the degradation evolution and the transformation of the contact topographies. Finally, the comparison between deep-groove ball bearings and roller bearings is discussed.

2. Roller bearing damage evolution

In order to recover the evolution of the bearing life, endurance tests have been performed on a dedicated test bench, and then interrupted tests has been done on each identified phases of the bearing life. In order to compare the wear evolution between ball bearings and roller bearings, the experimental protocol and the test parameters have been kept constant, with respect to previous works [5] [6] [8] [22] [25].

Here, the experimental tests have been carried out on single row spherical roller bearings, with a pitch diameter of 17.1 mm and a roller of (maximum) diameter of 4.7 mm and length of 5.5 mm (Figure 1-a). The rings and rollers are both made of 100Cr6 steel. The bearing is 100% filled with an aeronautical grease Aeroshell 33.

The tests have been performed on a SKF test bench, named “R2”, schematically represented in Figure 1-b. The set-up is conceived to apply high radial load on the bearing outer ring and oscillatory motion on the inner ring, which rotates with the shaft. The oscillatory motion is assured by a crank-rod system, actuated by an electrical engine. The radial load is applied using dead weights and a lever arm. A more detailed description of test bench can be found in [6].

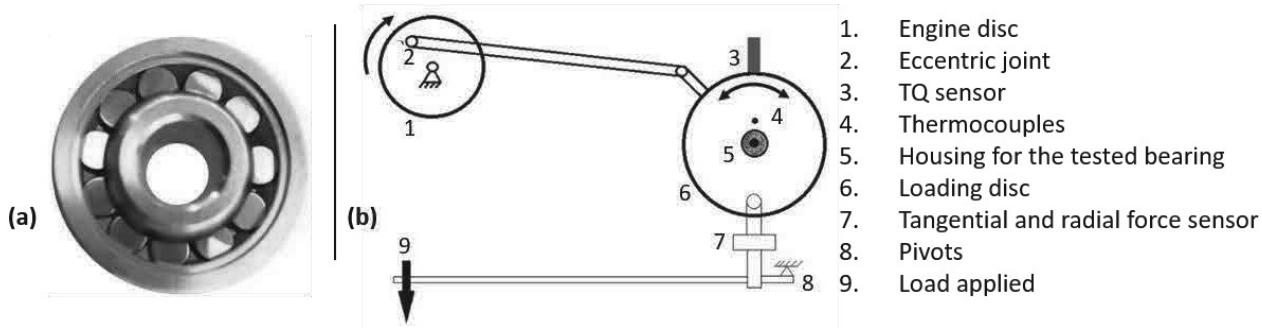

Figure 1: tested bearing and scheme of the test bench "R2".

Applied on the inner ring, the oscillation motion of an amplitude of ± 20° avoids overlapping of the rolling traces and then simplifies the interpretation of the surface observations. In order to accelerate bearing ageing without overheating of the contact, the oscillation frequency is set to 5 Hz.

On the bearing outer ring, the radial load is applied by dead weights and maintained at a constant value of 10 800 N. This load is set in order to obtain a maximum contact pressure of 4 GPa [5]. The load is supported by the roller situated at the top of the tested bearing (Figure 2,Table 1). The number of rollers that support the radial load depends on the bearing geometry. During the oscillating cycle, the magnitude of the radial load varies between a minimum and a maximum value as a function of the rolling element instantaneous position. Figure 2 shows the theoretical static radial load distribution between the rolling elements. In addition, the name of the most loaded rollers and the respective rolling marks are indicated. In Figure 2, Ri and Tj indicate respectively the i-th Roller and j-th rolling Trace. Table 2 summarizes the test parameters.

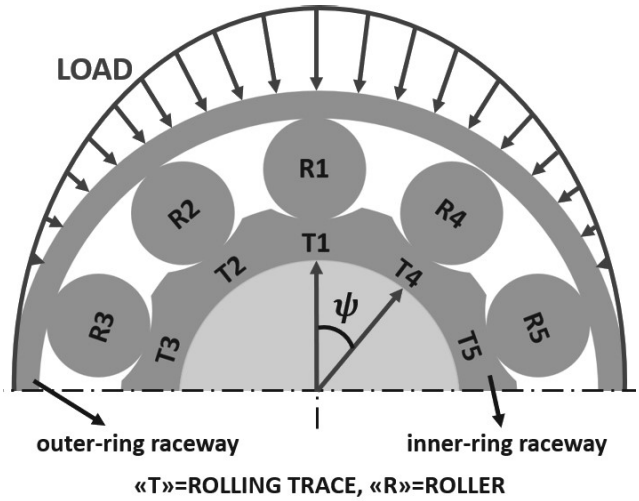

Figure 2: internal load distribution and definition of the most loaded traces and rollers.

angular position, [°]	Static radial load, [N]	(%) of the total radial load
0	4 000	37
±32.7	3 303	31
±65.4	1 512	14
±98.1	0	0
±130.8	0	0
±163.5	0	0
±180	0	0

Table 1: radial load distribution in function of the angle ψ.

Lubricant	Aeroshell grease 33
Level of lubrication	100% filled
Radial static load applied	10 785 N
Motion type	Oscillatory motion
Amplitude of the oscillatory motion	40°
Oscillation frequency	5 Hz

Table 2: test conditions.

Three main sensors are used to follow bearing evolutions during the whole test. A proximity sensor ("TQ sensor" in Figure 1) model TQ-401 (VibroMeter® Meggitt SA, Fribourg, Switzerland) to measure the relative displacement between the inner and the outer rings (RD). A bi-axial force transducer (model FX2-2, SIXAXES SA, Argenteuil, France) to record the resistant torque (RT) and the normal load. And then a thermocouple touching the outer ring surface to prevent overheating.

A set of endurance test was performed on roller bearings and, among them, two tests are presented here, corresponding to the two possible life evolutions recovered during the tests. Figure 3 shows the resistant torque (RT) and the relative displacement (RD) measured during two different tests until the set limit of the

resistant torque is reached (bearing end of life). The resistant torque is a result of the local frictional interaction, the rolling element kinematics and the surface evolution. The local friction coefficient of the greased contact, for new surfaces, has been measured on a dedicated tribometer and has been estimated at about 0.1. The curves have been normalized along the x-axis with respect to the duration of each single test. The relative displacement between the two rings is measured along the radial (loading) direction, and an increase of its value (reduction of the gap between the rings) corresponds to a degradation of the rolling interfaces.

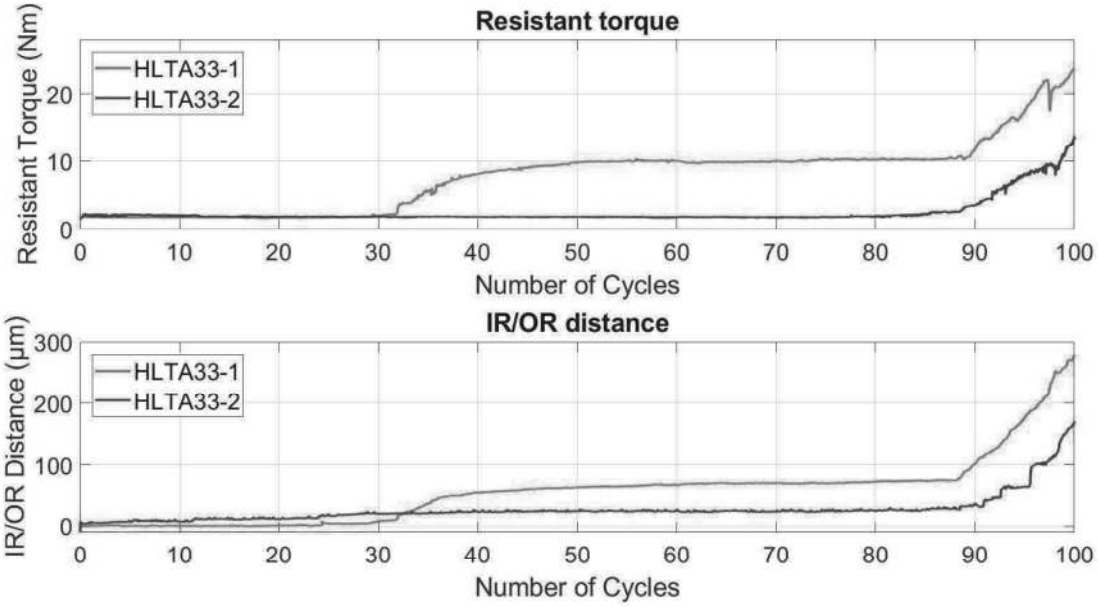

Figure 3: RT and RD normalized curves of lifetime tests.

TEST	CYCLES
HLTA33-1	46 053
HLTA33-2	116 759
HLTA33-3	209 925
HLTA33-4	148 499

Table 3: lifetime tests.

The tested bearings have shown a very different life duration. Nevertheless, the tested bearings show common trends in the curve of the RT and RD curves, corresponding to a reproducible evolution of the bearing degradation scenario. The schemes of the two possible scenarios of the evolution of the RT and RD curves, during the overall bearing lifetime, are presented in Figure 4. The main common points of lifetime tests are:

- The presence of a running-in phase;
- The presence of a first plateau, i.e. a steady-state phase, where the value of the RT remains constant;

- The presence of a relative fast increase of the RT in the final part of the bearing life, which leads to its end.

On the contrary, a difference has been identified in the possible presence of a second steady-state phase, after the first plateau and just before the fast final increase of the torque, point 5 in Figure 4.

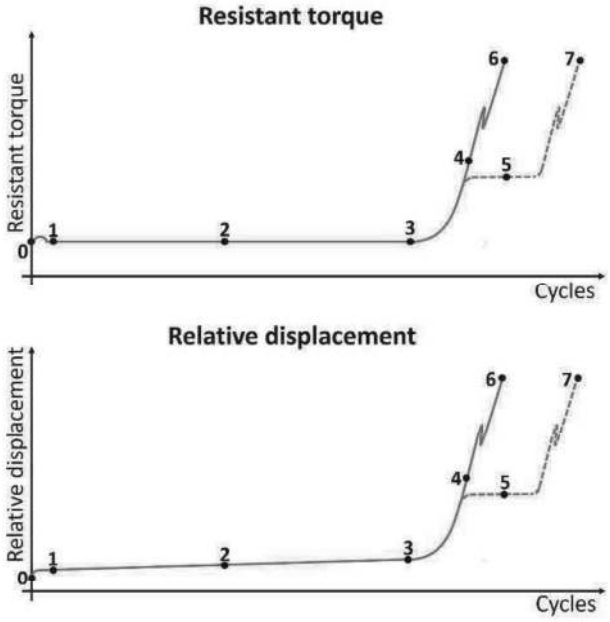

Figure 4: Wear model of RT (up) and RD (down) for a greased roller bearing.

In Figure 3, the different ageing step can be identified. At the beginning of the test, from point 0 to point 1 (Figure 4), the RT increases slightly before decreases again. This transitory represents the running-in phase and it lasts on average approximately 1,000 cycles. After, from point 1 to point 3 (Figure 4) the signal stabilizes, there is the main steady-state phase where the RT amplitude remains constant. This stationary phase is interrupted at the point 3 (Figure 4), when the amplitude starts to increase in a faster way. At the end of this first plateau and after the increase in the RT, two possible scenarios occur. In one case, a second steady-state is present, point 5 (Figure 4), followed by a further increase leading to the final damage. In the other case the RT continues to increase quickly to the end of the bearing life, without the second plateau. In the final phase of both cases, a sudden decrease and subsequent increase in the signal is present.

Starting from this scheme, interrupted tests have been carried out in order to understand the accommodation mechanisms involved during each step. The following phases of the degradation scenario have been analyzed:

- running-in, from point 0 to point 1 (Figure 4);
- first steady-state, from point 1 to point 3 (Figure 4);
- damage initiation, from point 3 to point 4 (Figure 4);
- second steady-state, around the point 5 (Figure 4);

- damage growth and bearing end of life, from point 5 to point 7 or point 4 to point 6 (Figure 4).

At each point, loaded rollers and inner ring raceway have been analyzed with a SEM, Scanning Electron Microscope (model FP 2014/23 QUANTA 600, FEI, Brno, Czech Republic).

3. Surface topography evolution

In this section the evolution of the surface topography in the key points of the curves, shown in Figure 3, will be presented. Surface topography analysis has been analyzed using a SEM and because stresses at the outer-raceway contact are lower (due to the concave contact), the contact of the roller with the inner-ring will be focused.

The analysis of surface topography will be supported by the results of numerical simulations. A 3D finite element model has been developed and solved using a commercial code. Because of the high computational effort due to the contact non-linearities, the analysis is focused on the most loaded roller, taking in account the inner and outer ring sectors. Moreover, fine meshing, of about 10 μm size, has been developed at the contact surfaces, ensuring a reliable distribution of the contact stress and strain. Based on an elastic-plastic material behavior, the numerical simulation consists in a loading phase followed by the simulation of a cycle of oscillation of amplitude ±10° and characterized by a frictional coefficient defined experimentally and equal to 0.1. A static analysis has been performed with a ramp of the loading force on the outer ring and the oscillation imposed at the inner surface of the inner ring, as imposed into the experiments by the oscillation of the shaft. The reader is referred to reference [5] for the details on the numerical approach.

3.1. Initial surface topography

The point 0 (Figure 4) corresponds to a new bearing. Figure 5 presents the topographies of the inner-ring raceway and the rollers. They are the reference topography of the contact surfaces, needed for the understanding of the superficial evolutions. The roller and the inner ring raceway present a different initial topography, due to different machine processes. As shown in Figure 5, the raceway surface presents regular and parallel machining grooves while the roller presents a smoother surface with several local superficial defects.

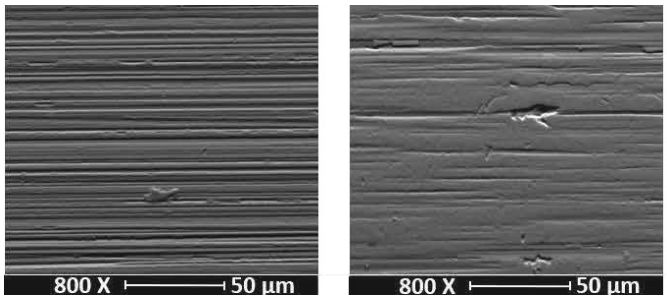

Figure 5: Initial topography of a roller bearing. Inner-ring (left) and roller (right) SEM analysis. Mode: TOPO.

3.2. Running-In

From point 0 to point 1 (Figure 4), the running-in represents the initial part of the bearing evolution scenario. From the RT signal, we can distinguish the running-in phase in two steps:

- Macroscopic running-in. The inner ring track shows macroscopic plastic deformation (Figure 6a, Zone 2) and the contact between raceway and rollers becomes more conform, increasing the bearing resistant torque and producing a decrease of the ring distance. The contact pressure, calculated by the 3D elasto-plastic model, ranges between 3 and 4.5 GPa during the bearing oscillation, along the highest loaded contact trace between roller and race.
- Microscopic running-in. In this phase the interaction between the third and the first bodies lead to the plasticization of the machining grooves [6] [25]. A smoother area starts to appear (Figure 6a, Zone 1). This stage of running-in provides a slight decrease in the RT.

Considering the most loaded roller ("R1"), the analysis of surface topography shows the presence of rolling (local sticking) and sliding contact regions are well recognizable. In Figure 6b, numerical results concerning the state of the contact and the microscope observations are superimposed. The extension and location of these areas are confirmed.

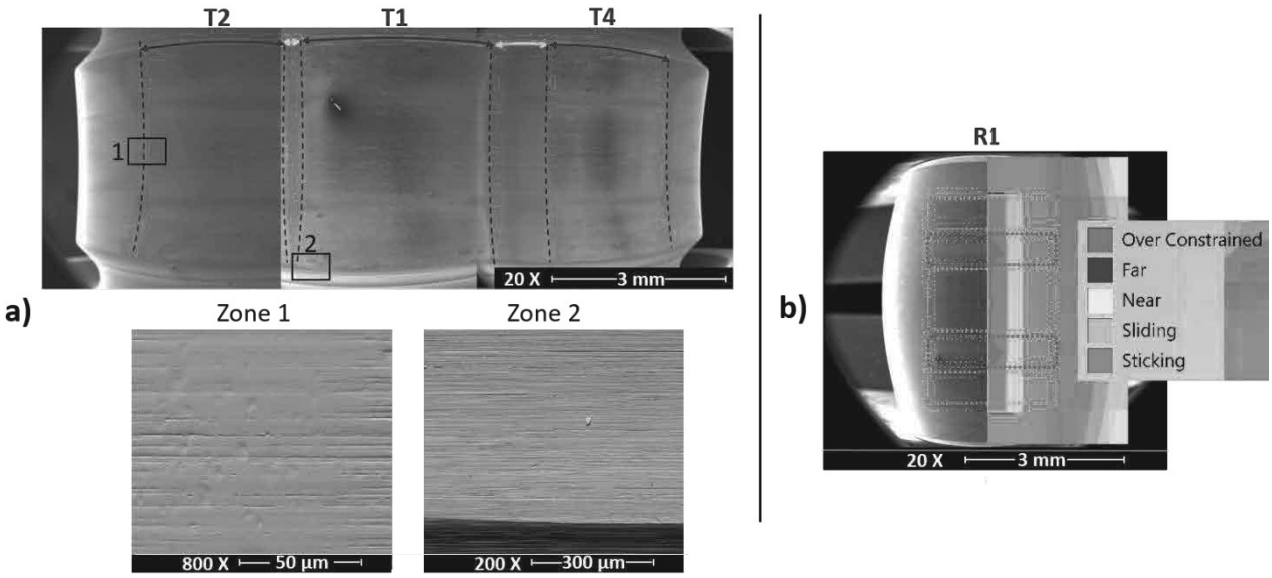

Figure 6: a) End of running-in: SEM analysis of the inner ring (Mode: SE), with zooms on different zones in the in the contact area (Mode: TOPO). b) Roller contact status (Mode: SE).

At the end of the running-in phase, the inner-ring and the most loaded roller present still signs of machining grooves.

3.3. Steady state (central phase)

During the first phase of steady state period from point 1 to point 2 (Figure 4) where the RT and RD curves are stable, the contact surfaces stay stable without significant modification on the macroscopic topography (Figure 7 and 8). This explains the stability of the RT and RD curves. During that phase, at specific locations, the morphology of contact surfaces becomes smoother (Figure 7) which might imply the formation of a plasticized layer recovering machining grooves. During the first part of steady-state phase the asperities of the most loaded traces of the inner-ring interact with the roller and the grease, producing in some zones (Figure 7, Zone 1&2) a smoother topography. These smooth plasticized areas might result from the interaction of the inner ring, rollers and the grease. According to previous work on deep groove ball bearing [6]and hybrid bearings [25], this smoothed area could allow a lower rolling resistance torque and protect the contact surface from further degradation, leading to a long steady state phase.

The most loaded roller has an unchanged topography compared to the running-in phase.

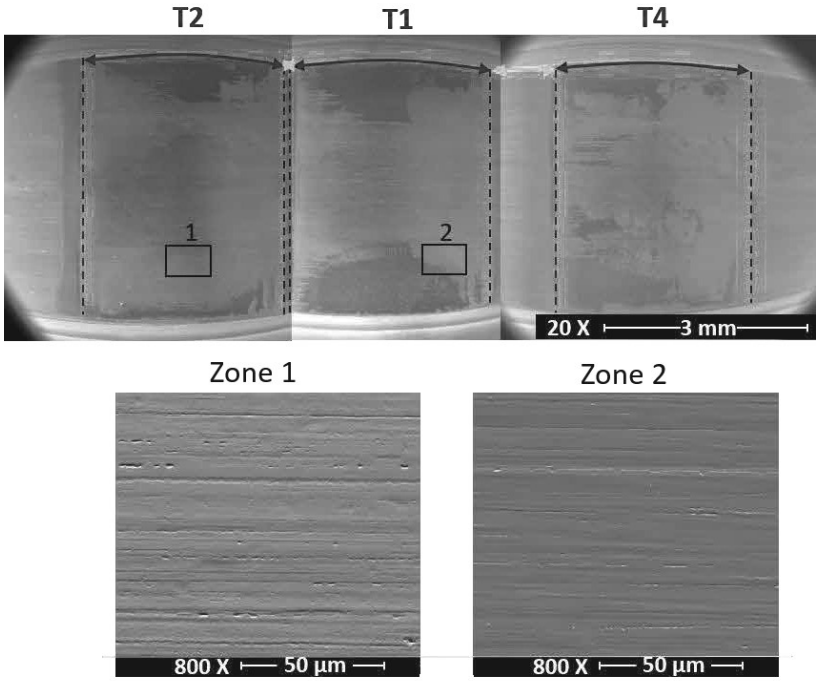

Figure 7: Central part of steady-state phase: SEM analysis of the inner ring (Mode: SE), with zooms on different zones in the contact area (Mode: TOPO).

3.4. Steady state (final phase)

During the second part of the steady state period, from point 2 to point 3 (Figure 4), the smoothed areas [6] [25] are developed in a striking way on the areas between the traces, where the higher sliding ratio occurs with a local source and accumulation of wear particles (Figure 8, Zone 1).

On the contrary, the most loaded roller, where lower sliding ratio and lower particle accumulation occurs, has an unchanged topography compared to the running-in phase (Figure 8, Zone 2).

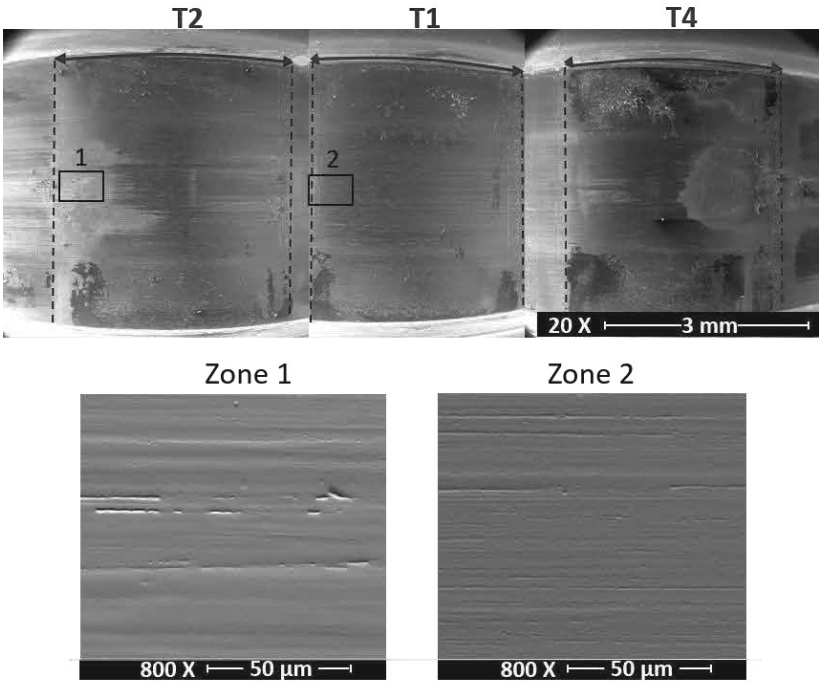

Figure 8: Final part of steady-state phase: SEM analysis of the inner ring (Mode: SE), with zooms on different zones in the contact area (Mode: TOPO).

3.5. Damage initiation

At the end of the steady-state phase, after the point 4 (Figure 4), macroscopic damage wear process starts, and the RT increase rapidly. The observations of the inner-ring (Figure 9) shows the detachment of macroscopic slices of material (Zone 2), just after the increase of the RT (point 4, Figure 4). In this case, as shown in Figure 8, the detachment of material affects a large part of the raceway track.

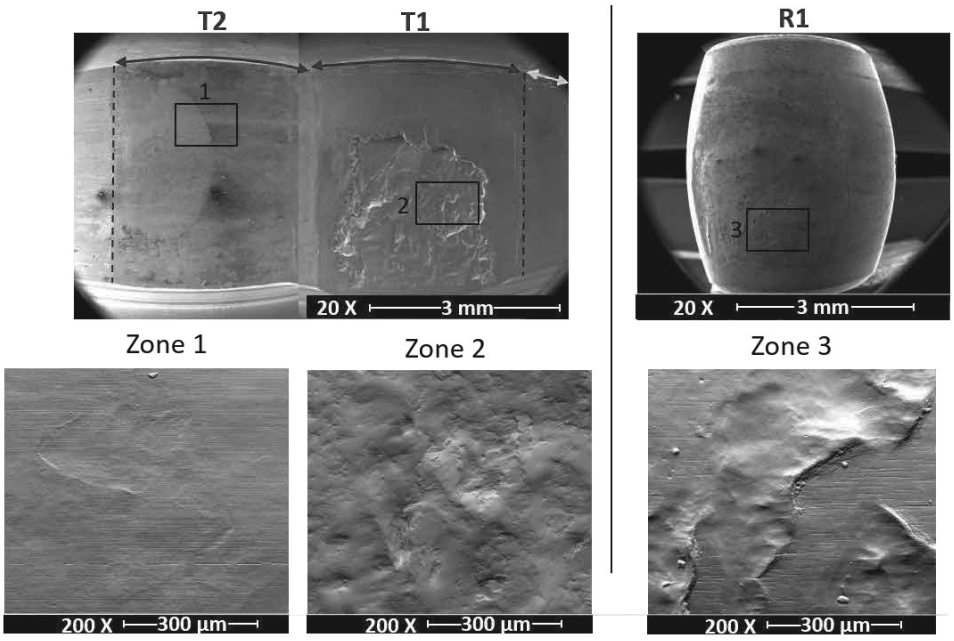

Figure 9: Damage initiation: SEM analysis of the inner ring and roller (Mode: SE), with zooms on different zones in the contact area (Mode: TOPO).

Traces 2 and 4, adjacent to track 1, do not show any damage, but only macroscopic plastic deformations of the surface (Zone 1, Figure 9), due to the macroscopic wear particles coming from the detachment on the track 1. They are those where the expansion of a smooth morphology is the most relevant too, maybe they are better protected.

The observation of the ring and roller surface topography leads to the statement that the inner ring is the first to be damaged. The increasing of the inner ring damage causes as well the initiation of the roller damage, which starts to show a very worked surface (Zone 3, Figure 9). This is due to the rolling of the roller on a highly irregular surface of the damaged raceway.

3.6. Second steady state

After the damage accumulation phase, two different scenarios are possible:

- 1st scenario: either the most loaded rollers and raceway tracks begin to highly damage very quickly, bringing to a fast end of the bearing life
- 2nd scenario: or the modification of contact geometry continues until a new contact equilibrium state is established. In that second scenario, the second steady state may occupy a relatively short number of cycles because of the bad contact conformity. Then, the bearing degradation increases exponentially again, up to the bearing end of life. The second scenario lead to the point 7 of the Figure 4.

Figure 10 shows how, in this 2nd degradation scenario, the damage on the inner ring track is smaller than the one in the previous case. The extent of detachment of material on Track 1 can affect the appearance (or not) of a second stationary phase. In this case, considering the smaller extent of the damage, the roller can easily plasticize the irregularities on Track 1 and a new equilibrium state is reached.

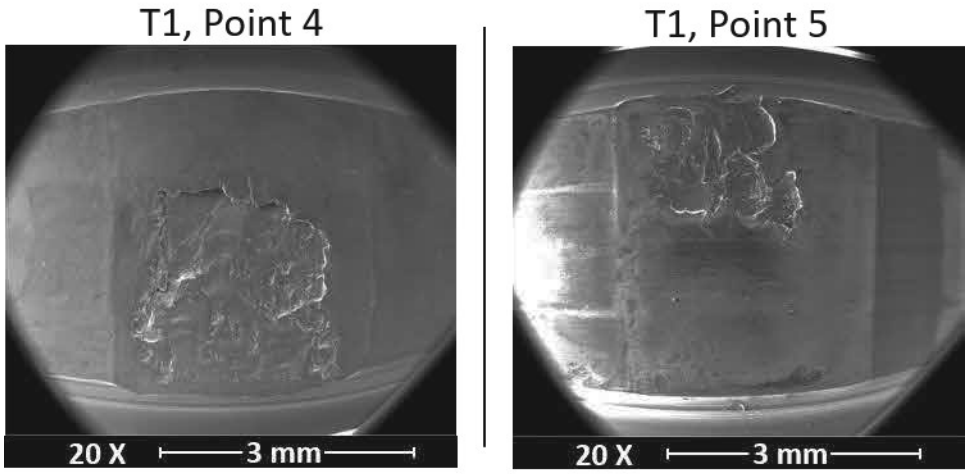

Figure 10: comparison of material detachment on trace 1 between the two different scenarios.

While the roller showed slight changes up to this stage, the beginning of the damage of the track with the consequent detachment of material involves a modification of its topography. Due to a bad conformation

of the roller and the raceway, high pressures seem help to develop a smooth area on the roller (Figure 11), with a similar topographical aspect of the one previously formed on the raceway surface (Figure 7).

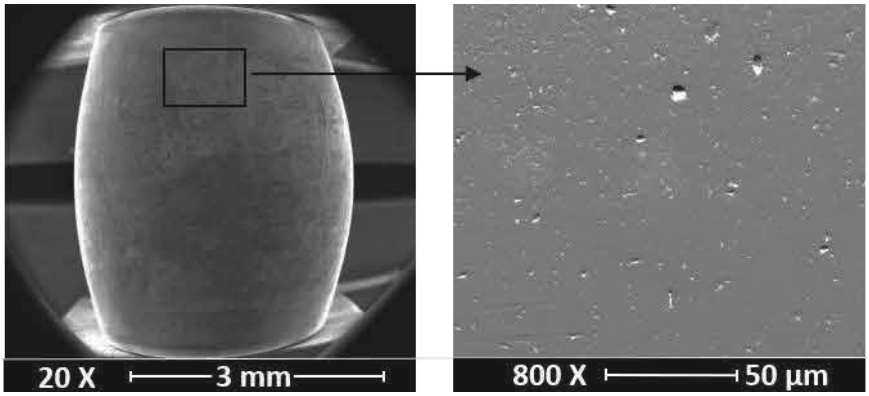

Figure 11: Second steady-state: SEM analysis of the most loaded roller (Mode: SE), with zoom in the contact area (Mode: TOPO).

3.7. Damage growth and bearing end-of-life

During the last part of the bearing life (between point 4 and 6 or 5 and 7), the irregularities on the damaged inner ring continue to evolve (Figure 12), and the RT and RD curves have an exponential trend up to the torque limit, corresponding to the bearing end of life.

At the end of the bearing life the contact surfaces and geometry are completely damaged (Figure 12), explaining the sudden increase of the RT and RD curves.

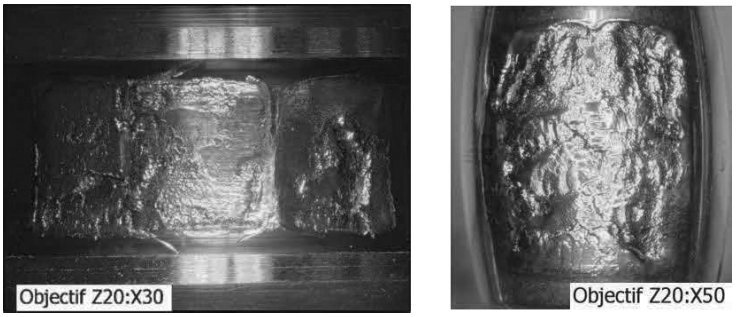

Figure 12: End of life: Optical microscope analysis of the inner ring (left) and roller (right).

4. Accommodation mechanisms and bearing degradation scenario

The analysis of the contact surfaces during the different phases of the bearing life allowed for the different accommodation mechanisms at the interfaces to be reconstructed. The local contact stress and relative velocities at the interfaces are accommodated in different ways, as a function of the contact zones. In particular, the ratio between local sliding and sticking (Figure 6) can bring to either the detachment of wear particles from the initial topography (machining grooves) or the compression/plasticization on the superficial layer.

Among the accommodation mechanisms that seem to allow for a stability of the bearing interface at high contact pressures, the formation of smoothed area has been identified. From the observation of the sites where this takes place, two main factors can be assumed: the combined presence of local sliding & rolling and the presence of wear particles in situ. The bearing working condition seems to be at the origin of this superficial evolution [26], which accommodates the high contact stresses and allow for the establishment of a long steady state in the operative life of the bearing.

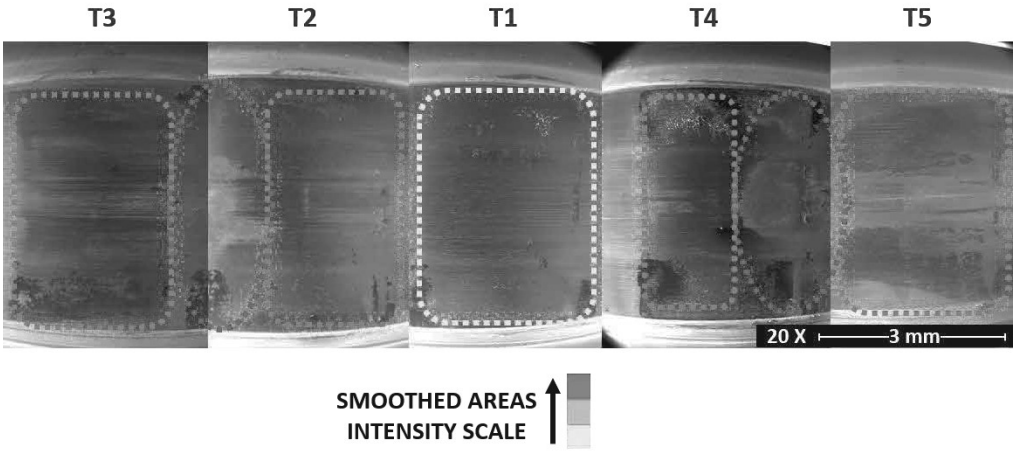

Figure 13: scheme of zones where smoothed plasticized areas developed with a qualitative scale of its formation.

The smoothed areas are formed on both the raceway and roller surfaces. However, the damage of the bearing is initiated at the raceway, and more precisely at the Trace 1. This seems to be a consequence of the less smoothed surface on this trace, with respect to the adjacent ones. Figure 13 shows the distribution of the phenomena observed on the overall raceway. This difference in the forming of the smoothed area is due to both the lower amount of sliding, bringing to lower source of wear particles in situ, and the expulsion of the particles toward the adjacent traces. Figure 13 shows how the more smoothed surface corresponds to the areas on the borders of Traces 2 and 4, where the wear particles agglomerate.

On the other side, the lower sliding at the Trace 1 is demonstrated by the observation of the lateral surfaces of the roller (Figure 14). The Figure shows scuffing marks at one side of the rollers. Nevertheless, for the Trace 1 the marks are localized only along the oscillating angle, showing the absence of overall sliding of the roller. On the contrary, the scuffing marks cover all the circumference of the roller R2 and R4, showing an overall sliding of these rollers the respect to the corresponding contact traces.

Moreover, the observation of the roller sides allows for highlighting an asymmetry in the contact, due to the bending of the shaft under the radial load. This observation can justify as well the large scattering of the endurance tests (Figure 3), due to the bearing misalignment and the corresponding distribution of the contact stresses.

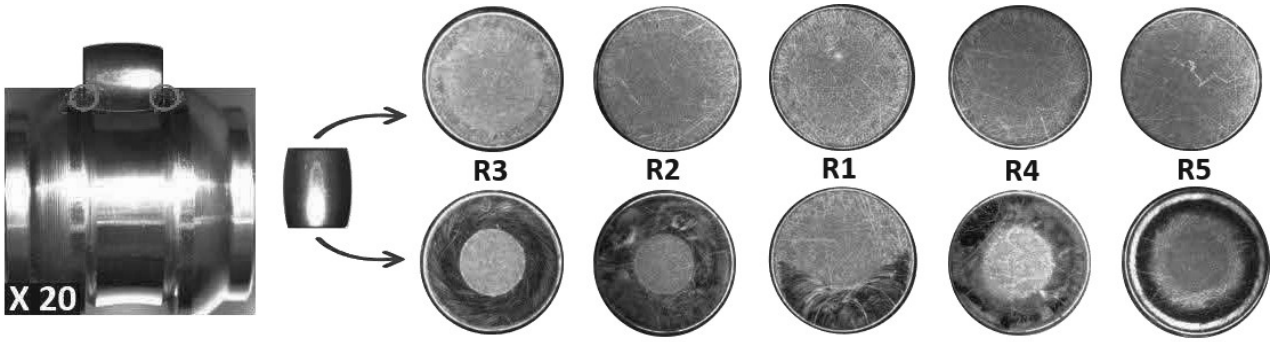

Figure 14: scuffing marks on each face on the most loaded rollers.

When focusing on the damaged trace (Trace 1), the initiation of the damage on the raceway, instead of the roller, is in agreement with the results from the numerical simulations. Figure 15 shows the observation of the damage initiation, when the test is stopped at the second steady state after the first damage occurs (Figure 15- right), and the numerical results on the residual plastic strain distribution (Figure 15- left), on both the roller and the raceway. The numerical results show a higher plastic deformation on the surface of the inner ring raceway with respect to the roller surface. Moreover, the contact zone showing the highest plasticization, due to higher shear stress, is the one close to the borders of the contact race (green and yellow areas in the Figure 15, top left). This is the same zone where the detachment of the superficial material first occurs (Figure 15, top right), showing how the numerical simulation predicts correctly the areas where the concentration of stresses and strains brings to the initiation of the damage.

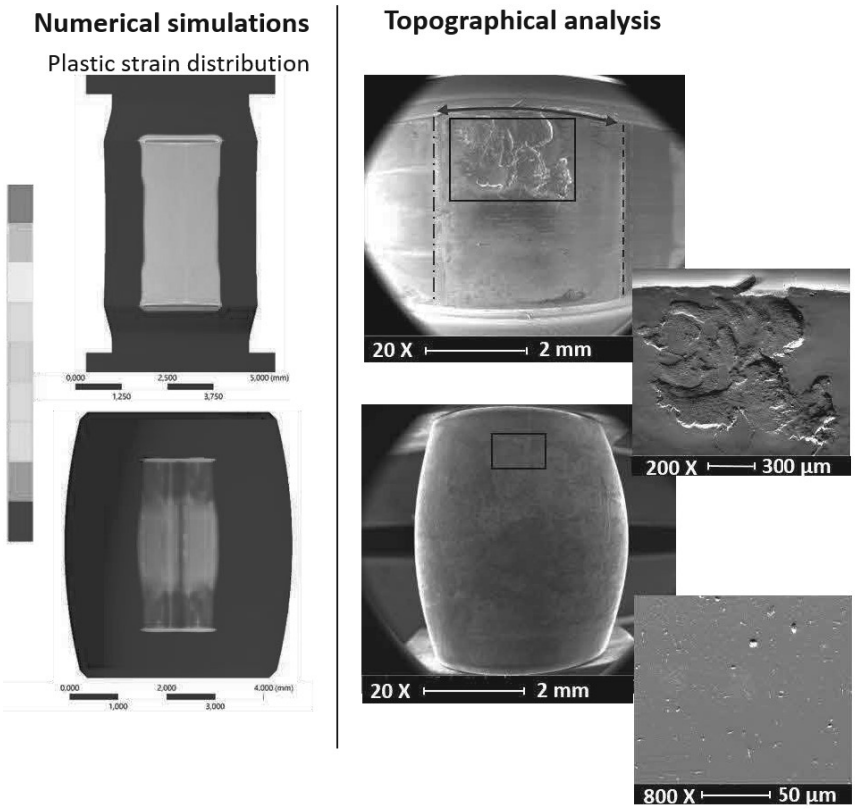

Figure 15: Comparison between numerical results (Equivalent Plastic Deformation) and experimental results (Topographical analysis).

5. Roller bearings versus deep-groove ball bearings

The results obtained in this study on roller bearings are here compared with those from previous studies, focused on deep-groove ball bearings subjected to the same boundary conditions [5] [6] [8] [22] [25]. The two bearing types have different geometrical dimensions, a different kind of rolling element, but are made of the same material (steel 100Cr6). The grease type and lubrication level applied in the endurance tests are the same. For the both, the experimental tests have been performed on the same "R2" SKF test bench. For the two cases, the tests have been conceived to guarantee the same contact pressure on the most loaded contact pairs and the same oscillatory motion. For the both analyses, the imposed oscillation amplitude is small enough to avoid overlapping of the rolling traces. The aim of the comparison is the investigation effect of the change in the geometry on the accommodation mechanisms and on the degradation scenario.

Figure 16 presents the models of the bearing life and the evolution of the surface topographies reconstructed for the roller bearing and the deep-grove ball bearing. Observation which can be made thanks to that comparison are:

1. In both cases it is possible to recognize five phases that characterize the bearings life; these have different duration, but in both cases, they represent precise and defined changes in both the contact surfaces and evolution of the signals.
2. Some recurring accommodation mechanisms take place. In particular, the creation of a smoothed topography in particular areas on the inner-ring raceway is observed (Figure 17). The smoothed areas are created in both cases during the steady state phase; however, while in ball bearings they are developed at the beginning of steady state (just after running-in), in roller bearing they appear clearly during the central phase. In the roller bearings, also the roller developed an evident zone with smoothed topography, which covers its surface after that the first damage of the raceway occurs, when superficial stresses and wear flows increase.
3. In the case of deep-groove ball bearing, the smoothed areas spread more uniformly at the center of the inner ring raceway. While in the case of roller bearing, traces 2 and 4 are preferential sites for such superficial transformations. In fact, in these two traces a higher sliding rate occurs with respect to trace 1. The two main aspects that could justify a different development of the smoothed topographies on different sites are:
    i. The geometry of deep-groove ball bearing. In fact, the inner-ring raceway is characterized by a deep-groove that allows to better accumulate the wear particles near the contact. The roller bearing raceway is more open and moreover there are grooves on the sides of the raceway, in which grease and wear particles can be accumulated, decelerating in this way the formation of the smoothed area.

ii. A greater sliding motion of the most loaded rolling element in deep-groove ball bearing than in roller bearing. This seems fundamental for formation of the smoothed areas. In fact, a greater sliding implies a greater plasticization and can accelerate in this way the superficial transformation, as showed by the attitude of forming a smoothed area at the border of the traces 2 and 4.

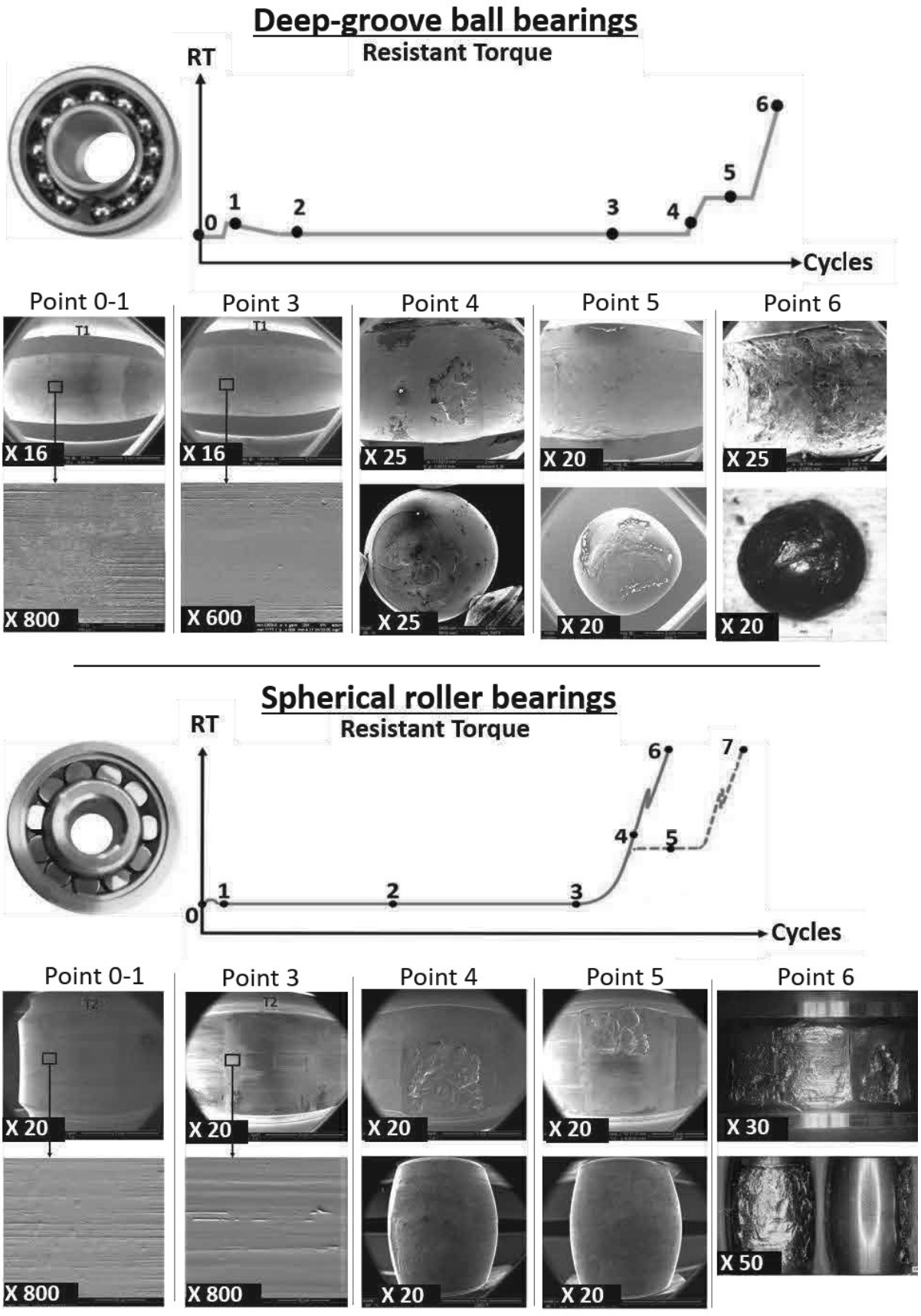

Figure 16: comparison of degradation scenario models.

4. a subsurface plastic strain accumulation, in the case of deep-groove ball bearings, is located on the most loaded ball (Figure 17) and brings the ball to damage first. On the contrary, in the case of

roller bearings the roller is not subjected to such failure mechanism, and the surface of the raceway is damaged first.

5. rollers can slide also on the flanges of the inner-ring raceway so there are other contacts in the roller bearing, which are not present in the deep-groove ball bearing. The scuffing marks analysis on the roller-ends allowed some hypothesis to understand the degradation scenario of the roller bearing:
    i. the presence of scuffing on one side of the roller highlights the misalignment of the bearing, which involves a change in the distribution of stresses.
    ii. The scuffing marks allows us to have information about the status of the investigated contacts. It was possible to notice how the roller 1 is characterized by pure overall rolling within the oscillation angle, while the adjacent traces showed overall sliding. A higher sliding/rolling ratio results in a higher local particle detachment, linked with the formation of the smoothed areas.

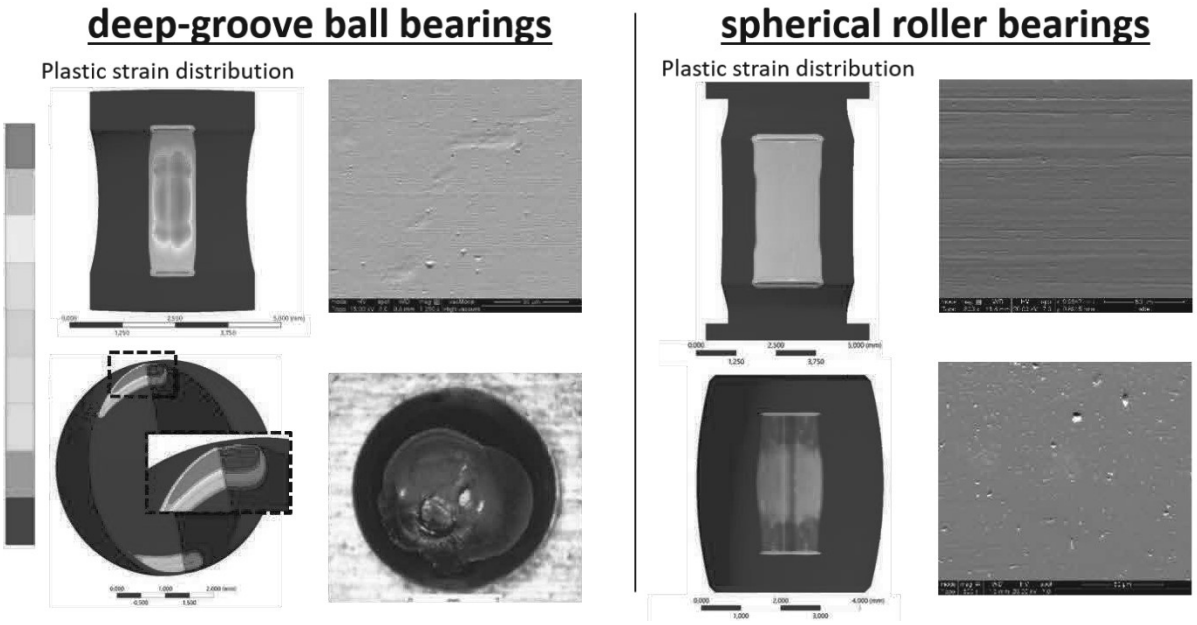

Figure 17: comparison of accommodation mechanisms between ball bearings (left) and roller bearings (right).

6. Conclusions

The evolution of greased spherical roller bearings under high load and oscillating motion has been investigated, by the analysis of the resistance torque and wear signals, together with the observations of the contact surfaces at the different life phases.

The reconstructed degradation model revealed five main phases, which characterize the greased roller bearings lifetime, under the tested loading conditions

The observation of the contact topographies, at the different phases of the bearing life, allows for providing a hypothesis on one of the main accommodation mechanisms. The generation of a smoothed area plays a key role in the bearing life by accommodating contact stresses and allowing for a long steady state in the bearing lifetime.

When comparing the roller and ball bearings, during the evolution of the bearing life, two main accommodation mechanisms can be identified: i) the strain accommodation within the TTS on the inner ring raceway surface; ii) the strain accumulation in subsurface, leading to fatigue cycles of the rolling element. The competition between these two accommodation mechanisms leads to the damage initiation on either the inner ring (in the case of roller bearing) or the rolling element (in the case of deep-groove ball bearing). The different geometry allowed as well for correlating the different accommodation mechanisms with the distribution of contact stresses and local sliding/rolling ratio.

References

[1] T. Harris, Rolling bearing analysis, 4th ed., Jhon Wiley & Sons, 2001.

[2] X. Ai and C. Moyer, "Rolling element bearings," *Modern Tribology Handbook: Volume One: Principles of Tribology,* pp. 1041-1093, 2001.

[3] F. Sadeghi, B. Jalalahmadi, S. Slack, N. Raje and K. Arakere, "A Review of Rolling Contact fatigue," *Journal of Tribology,* vol. 131, october 2009.

[4] L. Houpert, "A Uniform Analytical Approach for Ball and Roller Bearings Calculations," *Journal of Tribology,* vol. 119, no. 4, pp. 851-858, 01 October 1997.

[5] D. Tonazzi, E. Houara Komba, F. Massi, G. Le Jeune, J. Coudert and Y. Maheo, "Numerical analysis of contact stress and strain distributions for greased and ungreased high loaded oscillating bearings," *Wear,* Vols. 376-377, pp. 1164-1175, 2017.

[6] E. Houra Komba, F. Massi, N. Bouscharain, G. Le Jeune, Y. Berthier and Y. Maheo, "Experimental damage analysis in high loaded oscillating bearings," *Tribology international,* vol. 102, pp. 507-515, October 2016.

[7] P. Johns and R. Gohar, "Roller bearings under radial and eccentric loads," *Tribology international,* vol. 14, pp. 131-136, june 1981.

[8] F. Massi, N. Bouscharain, S. Milana, G. Le Jeune, Y. Maheo and Y. Berthier, "Degradation of high loaded oscillating bearings: Numerical analysis and comparison with experimental observations," *Wear,* no. 317, pp. 141-152, 2014.

[9] E. Booser and W. D.F., "Minimum oil requirements of ball bearings," *Lubrication Engineering,* vol. 9, pp. 156-158, 1953.

[10] A. Baker, "Grease bleeding-a factor in ball bearing performance," *NLGI Spokesman,* pp. 271-277, 1958.

[11] P. Lugt, "A Review on Grease Lubrication in Rolling Bearings," *Tribology Transactions,* no. 52, pp. 470-480, 2009.

[12] G. Morales-Espejel, P. Lugt, H. Pasaribu and H. Cen, "Film thickness in grease lubricated slow rotating rolling bearings," *Tribology International,* no. 74, pp. 7-19, 2014.

[13] P. Cann and A. Lubrecht, "An analysis of the mechanisms of grease lubrication in rolling element bearings," *Lubricaion Science,* vol. 11, no. 3, pp. 227-245, 2 March 2006.

[14] I. El-Thalji and E. Jantunen, "A descriptive model of wear evolution in rolling bearings," *Engineering Failure Analysis,* vol. 45, pp. 204-224, 2014.

[15] A. Voskamp, "Material response to rolling contact loading," *Jounal of Tribology,* vol. 107, no. 3, pp. 359-364, 01 july 1985.

[16] N. Raje, F. Sadeghi and R. Rateick, "A statistical damage mechanics model for subsurface initiated spalling in rolling contacts," *Journal of Tribology,* vol. 130, no. 4, december 2008.

[17] N. Raje, T. Slack and F. Sadeghi, "A discrete damage mechanics model for high cycle fatigue in polycrystalline materials subject to rolling contact," *International Journal of Fatigue,* vol. 31, no. 2, pp. 346-360, Febraury 2009.

[18] T. Slack and F. Sadeghi, "Explicit finite element modeling of subsurface initiated spalling in rolling contacts," *Tribology International,* vol. 43, no. 9, pp. 1693-1702, September 2010.

[19] J. Williams, "Wear modelling: analytical, computational and mapping: a contiuum mechanics approach," *Wear,* Vols. 225-229, pp. 1-17, April 1999.

[20] T. Harris and M. Kotzalas, Rolling Bearing Analysis, 5th ed., Taylor & Francis Group, 2006.

[21] L. Houpert, "Bearing life calculation in oscillatory applications," *Tribology Transactions,* vol. 42, no. 1, pp. 136-143, January 1999.

[22] Y. Berthier and D. Play, "Wear mechanism in oscillating bearings," *Wear,* vol. 75, no. 2, pp. 369-387, 15 January 1982.

[23] M. Renouf, F. Massi, N. Fillot and A. Saulot, "Numerical tribology of a dry contact," *Tribology International,* vol. 44, no. 7-8, pp. 834-844, July 2011.

[24] M. Godet, "The third-body approach: A mechanical view of wear," *Wear,* vol. 100, no. 1-3, pp. 437-452, December 1984.

[25] I. Ghezzi, E. Houara Komba, D. Tonazzi, N. Bouscharain, G. Le jeune, J. Coudert and F. Massi, "Damage evolution and contact surfaces analysis of high-loaded oscillating hybrid bearings," *Wear,* Vols. 406-407, pp. 1-12, 15 July 2018.

[26] A. Eleöd, F. Oucherif, J. Devecz and Y. Berthier, "Conception of numerical and experimental tools for study of the Tribological Transformation of Surface (TTS)," *Tribology Series,* vol. 36, pp. 673-682, 1999.